ARTICLE OPEN

Microstructured capacitive sensor with broad detection range and long-term stability for human activity detection

Xin He [1✉], Zhihao Liu[1,2], Gengzhe Shen[1,3], Xiang He[1], Jionghong Liang[1], Yu Zhong[1], Tianlong Liang[1], Jie He[1], Yue Xin[1], Chi Zhang[1], Dongdong Ye[4] and Guofa Cai [2✉]

In recent years, flexible stress sensors capable of monitoring diverse body movements and physiological signals have been attracting great attention in the fields of healthcare systems, human–machine interfaces, and wearable electronics. Inspired by the structure of natural eggshell inner membrane (ESIM), we developed a pressure sensor based on MXene ($Ti_3C_2T_x$)/Ag NWs (silver nanowires) composite electrodes and the micro-structured dielectric layer to meet the application requirements of wide detection range and long-term stability for the sensors. In the light of the nanoscale-microarray of the dielectric layer and the rough surface of electrode materials, this pressure sensor is expected to allow great and persistent deformation during the loading process. As a result, the device is characterized by an improved sensitivity, fast response (in the millisecond range), wide detection range (0–600 kPa), and long-term stability. The outstanding performance of the proposed sensor makes it possible to detect various human activities, such as speaking, air blowing, clenching, walking, finger/knee/elbow bending, and striking, demonstrating its good application prospects in wearable and flexible electronic devices.

INTRODUCTION

With the increasing demand for artificial intelligence and the internet of things, the potential of flexible and wearable sensors in human–machine interaction, soft robots, and health monitoring applications have received great attention[1–5]. According to the sensing mechanism, the flexible sensors are divided into four types: resistive-type[6–10], capacitive-type[11–13], piezoelectric-type[14–16], and triboelectric-type[5,17,18]. Among them, capacitive sensors have been intensively investigated owing to their characteristics of simple fabrication, good anti-interference, and excellent long-term stability[11–13,19]. However, their further applications are still restricted by the relatively low sensitivity and the sensing range[20,21].

To date, researchers have made lots of efforts to improve the comprehensive performance of the capacitive sensor in various aspects, such as sensitivity, detection limit/range, response time, and stability[12,22–24]. For example, introducing the microstructure has been regarded as one of the effective strategies for remarkably improving the sensor sensitivity due to the distinct deformation of the microstructure and the subsequent increase in the capacitance variation. Ma et al. reported a capacitive pressure sensor consisting of two electrodes and wrinkled polydimethylsiloxane (PDMS) dielectric layer. Compared with the sensor without a microstructure, the fabricated sensor exhibited improved sensitivity from 0.01 to 2.04 kPa^{-1} in the range of 0–2 kPa[24]. Additionally, bionic microstructures from natural plants, such as *aureum* leaf[25], lotus leaf[26], and rose petals[27] also have attracted much attention because of their delicate and green/cost-effective features. Guo et al. proposed a capacitive sensor consisting of a dried flower petal or a leaf sandwiched between two flexible electrodes. The device worked within a broad-pressure range

(0.6–115 kPa), the maximum sensitivity of which was 1.54 kPa^{-1}. Furthermore, compared with single-component electrode materials, such as carbon nanotubes (CNTs)[28,29], graphene[30,31], conductive polymers[32,33], metal nanostructures[34–36], and MXene ($Ti_3C_2T_x$)[37–40], the conducting composite has been widely utilized in the sensor electrode due to its combined advantages[41–45]. For example, the hybrid of one-dimensional (1D) and two-dimensional (2D) conducting materials could effectively prevent the aggregating and stacking of 2D material, thus forming a homogeneous connective network, which leads to good mechanical and electrical properties of the sensor electrode. Liu et al. reported a dendritic-lamellar MXene/carbon nanotube/polyvinylpyrrolidone electrode with high flexibility. The fabricated tactile sensor based on the composite electrode exhibited fast response, demonstrating for voice recognition and pulse measurement[45].

However, the diverse applications require the pressure sensors to not only respond to a small stimulus but also work under an ultrahigh load[9,46]. For example, the huge impact force coming from a sudden striking usually exceeds hundreds of kilopascals, which is likely to cause the overload or failure of the sensors. Therefore, apart from high sensitivity and fast response, it is highly desirable to ensure a wide detection range and long-term stability of the device.

Herein, we reported a capacitive sensor whose overall performance was improved by designing the microstructure of the dielectric layer and selecting composite materials of the electrode. Inspired by the natural microstructures, we utilized the eggshell inner membrane (ESIM) as the template of the PDMS dielectric layer. Compared with other templates, the unique fibrous ESIM provided the nanoscale- template with a more elaborated microstructure[47]. We could achieve abundant micro-
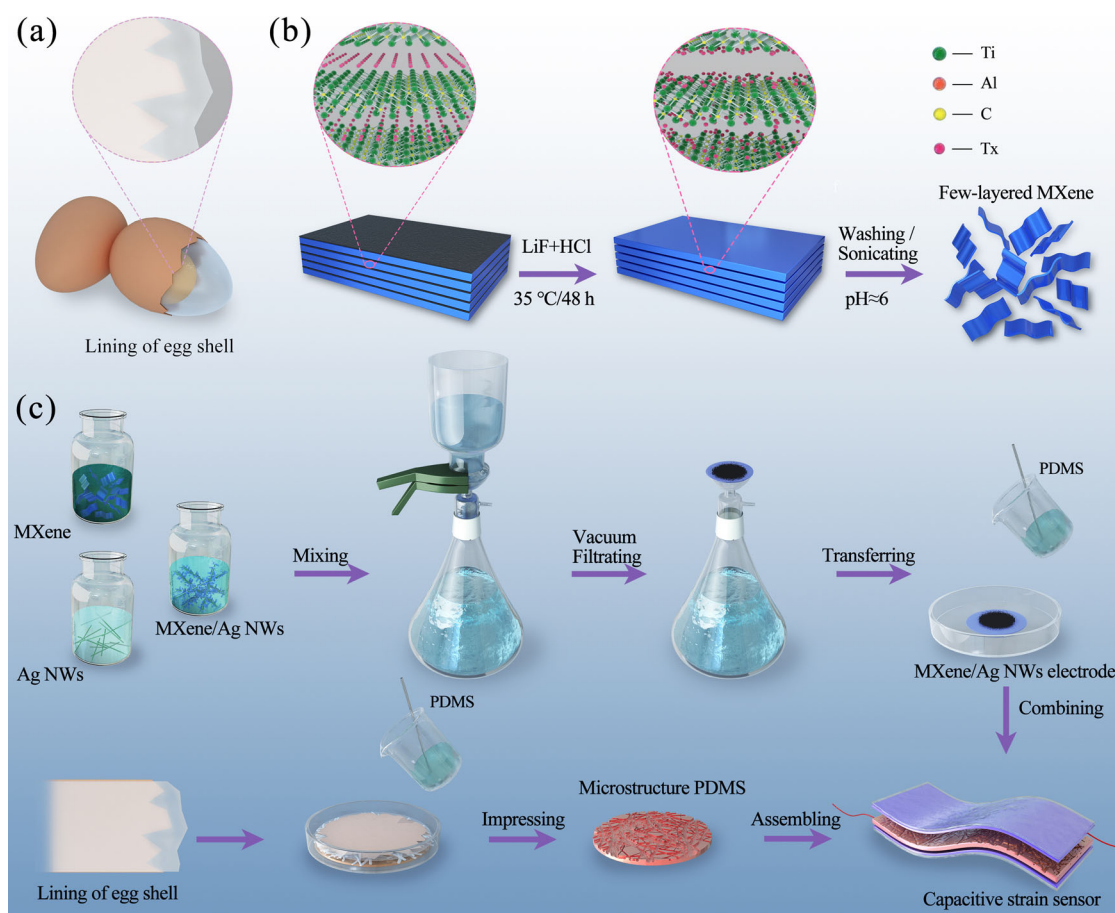
Fig. 1   Fabrication of the capacitive pressure sensor. a Structure illustration of the ESIM; **b** Schematic presentation of the fabrication process of MXene sheets; **c** Fabrication process of flexible capacitive pressure sensor.

fluctuations from the ESIM, which contributes to the remarkable deformation of the PDMS dielectric layer under the external stimuli. In addition, we proposed a composite electrode based on 2D MXene sheets and 1D Ag NWs. The Ag NWs can effectively decrease the restacking of MXene sheets, forming abundant conducting tunnels to facilitate electron transfer within the electrode. The fabricated MXene sheets and Ag NWs are closely contacted due to the electrostatic adsorption, which makes the conductive network have a stable structure[48–53]. In this case, there is no relative slip between two conducting components even under high stress due to the tight combination, leading to a stable electron path within the conductive networks, which is beneficial to the long-term stability of the device under the repeated loading/unloading. As a result, the micro-structured sensor exhibited an improved sensitivity especially in the high-pressure range, broad detection range (0–600 kPa), low detection limit (<16 mg), the fast response time (in the millisecond range), long-term stability, and reproducibility.

RESULTS AND DISCUSSION
Micro-structured dielectric layer and composite electrode
To improve the detection range and long-term stability of the capacitive sensor, we used the micro-structured PDMS as the dielectric layer and MXene/Ag NWs as the rough electrodes. The microstructure of PDMS was replicated from the structure of the ESIM (Fig. 1a), and MXene sheets was prepared by etching the MAX phase and further delaminating (Fig. 1b, see Methods Section for details). The composite materials consisting of Ag NWs and MXene sheets within the electrode are expected to provide

good contact and abundant conducting paths. The flexible capacitive pressure sensor was assembled using the micro-structured PDMS dielectric layer sandwiched between two MXene/Ag NWs electrodes (Fig. 1c).

Differently magnified SEM images disclose that the membrane is composed of fibrous protein with an average diameter of about 1 μm, presenting an interconnected network structure. There were a number of open spaces among the protein fibers (Fig. 2a, b and Fig. S1). The inverted microstructure was successfully transferred to the PDMS surface (Fig. 2c, d). These rugged inverse structures and the PDMS with small modulus could cause a wider range of compression deformation, which was expected to greatly improve the sensitivity and detection range of the sensor. The morphology and composition of electrode materials were further investigated. Figure 2e suggests that the MXene after etching features a multilayered structure. The element mapping illustrates that C, Ti, O, and F elements uniformly distribute across the multilayered MXene (Fig. 2f). As confirmed in the AFM image (Fig. 2g), MXene with a few layers was further acquired by ultrasonic treatment. The height distribution of MXene is about 5 nm, which is equal to 4–5 layers of $Ti_3C_2T_x$ nanosheets stacked together (Fig. 2g, h)[54,55]. The obtained MXene sheets can be completely filtered to form an intact and smooth film due to the stacking (Fig. S2). The inset of Fig. S2 indicates that the MXene sheets uniformly disperse in water without obvious agglomeration. In addition, the average size of the MXene sheets is ~100 nm, which is similar to the diameter of the prepared Ag NWs (Figs. S3 and 2i). The 1D Ag NWs were tightly wrapped by the 2D MXene sheets after the combination of the two conductive materials (Fig. 2j), supplying an improved surface roughness of the electrode. XRD
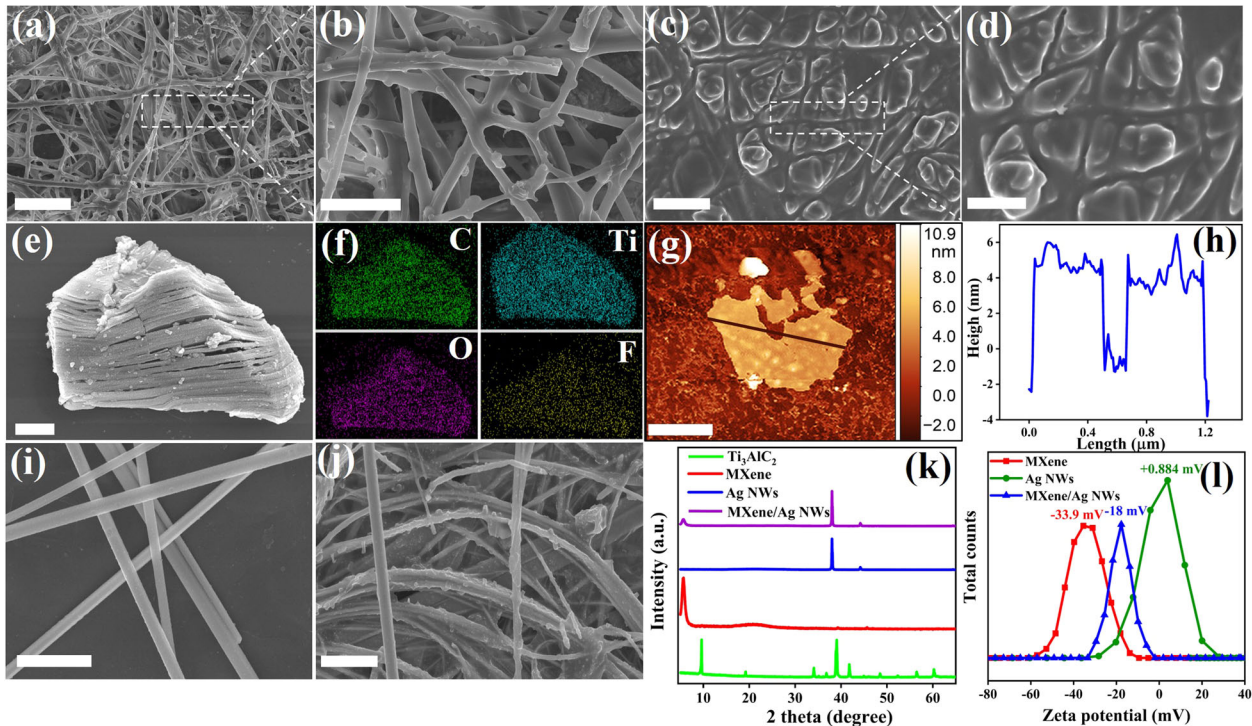
Fig. 2 Morphologies and structure characterization of the electrode materials. a–d SEM images of the ESIM, the PDMS dielectric layer with an inverted microstructure, the scale bars in (**a**) and (**c**) are 20 μm, that in (**b**) and (**d**) are 10 μm; **e**, **f** SEM image and its corresponding element mapping of the multilayered MXene, the scale bar in (**e**) is 2 μm; **g**, **h** AFM image and the height distribution diagram of the 4–5 layer MXene, the scale bar in (**g**) is 500 nm; **i**, **j** SEM images of pristine Ag NWs and the composite, the scale bars in (**i**) and (**j**) are 1 and 2 μm, respectively; **k** XRD patterns of Ti₃AlC₂, MXene, Ag NWs, and MXene/Ag NWs composite; **l** Zeta potentials of MXene, Ag NWs, and the composite.

characterization proves that we have successfully constructed MXene and metallic silver composites (Fig. 2k). Compared with the original material of Ti_3AlC_2, the (002) diffraction peak of MXene shifted to 5.9° after etching because of an increase in the layer spacing.

Due to the presence of the surface functional groups, the as-prepared MXene sheets were negatively charged with a zeta potential of −33.9 mV (Fig. 2l), while the surface of Ag NWs presented a positive charge with a zeta potential of +0.884 mV. Thus, the MXene nanosheets could closely adhere to the surface of Ag NWs owing to their strong electrostatic interaction, which is consistent with the result of SEM in Fig. 2j. The self-assembled composite (Fig. S4) displayed a resultant zeta potential of −18 mV. In the composite system, 1D Ag NWs and 2D MXene sheets can be regarded as the steel bar and cement in the solid buildings, respectively. The tight combination of the two materials could supply definite and stable conductive paths in the networks. The synergy of the two components contributed to the rough surface and high conductivity of the electrode (Fig. S5).

Sensing performance of capacitive sensors

We evaluated the performance of the micro-structured and flat capacitive sensors. The sensitivity of the sensor was measured through the slope of the relative change in the capacitance signal versus the applied pressure curve. The change rate of the capacitance of the flat sensor was ~50% under 100 kPa, presenting relatively a low sensitivity of 4.37 MPa⁻¹ (Fig. 3a). Furthermore, the change in the capacitance of the flat sensor was almost saturated over 100 kPa. Remarkably, the micro-structured sensor could work with a wider range of up to 600 kPa. The sensitivity value was increased to 10.13 MPa⁻¹ within 100 kPa, and especially by 54.3 and 95.7 times within high-pressure ranges of 100–400 kPa and 400–600 kPa (Fig. 3b).

To identify the contribution of the microstructure to the sensor performance, we simulated the sensor models based on the micro-structured and planar dielectric layer for comparison, and then investigated the variation in the stress and deformation under various pressures by finite element analysis (FEA) (see Methods section for details). According to the definition of capacitance $C = \varepsilon S/4\pi k d$ (where ε is the dielectric constant, d refers to the distance between the two plates, k represents the electrostatic constant, and S is the area of the capacitor plate), the device capacitance can be changed conveniently by controlling ε, S, and d. To obtain a higher sensitivity of the sensor, the capacitance variation is expected to increase to the largest extent. Under a given load, the stress and deformation were uniformly distributed across the surface of the flat sensor because of the planar and continuous contact interface between the electrode and dielectric layer (Fig. 3c). Therefore, the deformation and the contact area were hardly changed in this case. The flat sensor exhibited high resistance to the external pressure, resulting in small structural compressibility, as well as few capacitance changes. When the deformation reached saturation, the capacitance turned to be a stable value, which is in accordance with the result in Fig. 3b. Thus, the sensing range of the flat sensor was limited to 100 kPa, characterized by low sensitivity and a relatively narrow sensing range.

The simulation result revealed that the micro-structured sensor experienced a higher level of deformation than the flat one under the same pressure due to the rough surface of the dielectric layer (Fig. 3c). Higher stress was concentrated on the bulges of the microstructure. As the external pressure exerted on the sensor increased, the contact area between the electrode and dielectric layer was gradually increased, while the distance between the two electrodes was decreased. Thus, the micro-structured sensor was able to present a larger capacitance variation under the same pressure, enabling higher sensitivity and a wider detectable range.
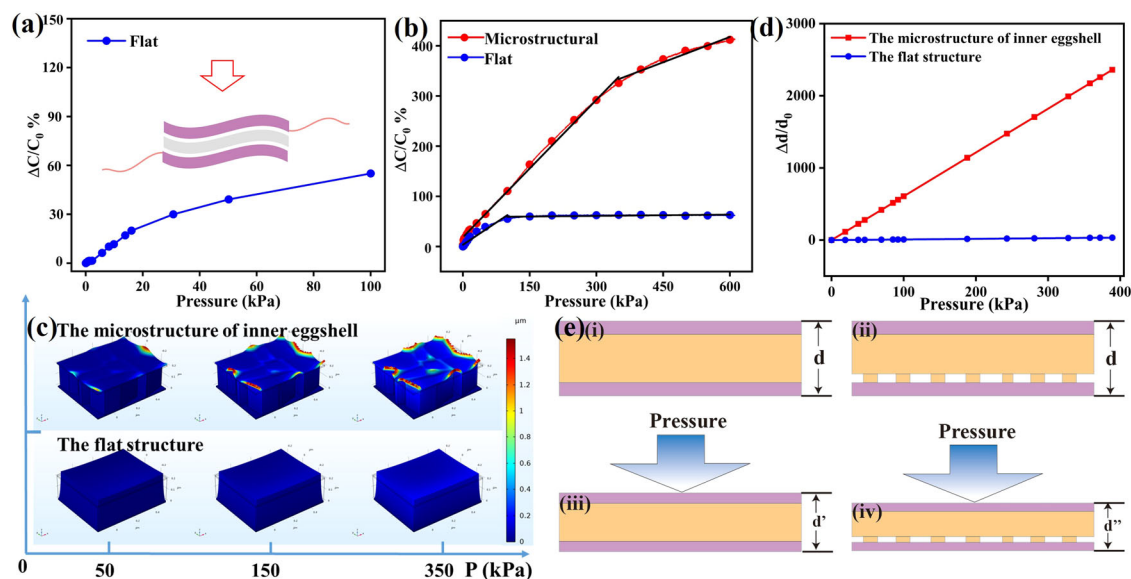
Fig. 3 Comparison of the flat and micro-structured sensors. a Capacitance changes of the flat sensor under the external pressure within 100 kPa; **b** Sensitivity comparison of the flat and micro-structured sensors within the range of 0–600 kPa; **c** Schematic diagram of the two sensors under the external pressure from Comsol simulation; **d** Compression displacement comparison of the two sensors; **e** Schematic diagram of the changes in the two sensors' distance and contact area under a given pressure.

In addition, the result of the simulated displacement between the two electrodes under various pressures and the structural changes of the capacitive sensors further proved that a larger deformation occurred under the same load in the case of the micro-structured sensor (Fig. 3d, e).

Therefore, the improved performance of the micro-structured sensor can be attributed to the following three aspects. First, the microstructure enables the sensor to experience a higher level of deformation under the same pressure, thus generating more obvious changes in the distance between the two electrodes, as well as the capacitance variations. Second, the high roughness of the electrode due to the combination of 1D and 2D conductive materials provides the improvement of the void space within the electrode. Thus, under a given loading, the stress sensor based on the MXene/Ag NWs electrode is expected to exhibit a large change in the d and C, and then generating a higher sensitivity coefficient (Fig. S6 shows the capacitance changes of the sensor based on smooth ITO/PET electrodes and the micro-structured PDMS dielectric layer, revealing a lower sensitivity within whole working range). Third, there is an air gap between each unit of the bulges in the microstructure. When the load was enhanced, the air gap would be gradually filled by PDMS material. Accordingly, the comprehensive dielectric constant ε of the dielectric layer rose ($\varepsilon_{Air} = 1$, $\varepsilon_{PDMS} = 2.5$–2.7), causing a larger capacitance change.

The instruments for testing the flexible pressure sensors included the push-pull machine, LCR capacitance measurement instrument, and program computer (Fig. 4a), while the important performance parameters for the stress sensors involved the response time and the detection limit. The time-response curve of the loading/unloading pressure indicated that the rise time and fall time of the micro-structured sensor was 280 and 290 ms, respectively (Fig. 4b). It is also worth noting that measuring the response time is limited by the movement rate (2.5 N/s) of the push-pull machine. Thus, the actual response time of the sensor could be less than 50 ms. We also tested the capacitance response of the sensor to rapid tapping using a finger, proving that the fast response within 50 ms (Fig. S7). A repeated signal can be recognized during the loading and unloading process of a grain of rice with a weight of 16 mg (Fig. 4c), denoting that the sensor can be used to reliably detect a subtle stimulus by the capacitive response. Additionally, the sensor showed stable signals in single

and multiple cycles under the pressures of 10, 20, 35, and 45 kPa, respectively (Fig. 4d, e). The response to each loading exhibited stepped waves and stable square wave-forms, revealing excellent sensing stability of the sensor within a wide pressure range. Moreover, the micro-structured sensor also demonstrated a precise response independent of the loading speed (0.10, 0.25, and 2.50 N/s) under the application of 2.5 N loading/unloading cycles (Fig. 4f). The rapid change and good recovery of the capacitance at each speed evidenced the fast response and excellent reversibility of the sensor.

To assess the reproducible sensing performance of the device, the sensor was loaded and unloaded with a constant pressure of 40 kPa dynamically for over 20,000 s at least (Fig. 4g). The micro-structured sensor exhibited remarkable robustness as the capacitance could recover its initial value even after being subjected to 1800 cycles. The magnified parts clearly showed no obvious amplitude change in the capacitance value at different loading/unloading stages (insets in Fig. 4g), verifying the excellent mechanical stability of the sensor. To confirm the potential for long-term application, the capacitance response of the sensor was further measured after 150 days under the same measuring condition (Fig. 4h, over 2700 cycles was shown in Fig. S8). The sensor still exhibited good stability over the whole period, and the capacitance variation was constant before and after long-term storage and measurement due to the stable conductive network within the electrodes. Furthermore, the SEM image of the dialectic layer after the repeated loading reveals that the PDMS microstructure cannot be destroyed (Fig. S9).

Demonstration of the micro-structured sensor

Based on the above characterizations and analyses, the flexible capacitive sensor demonstrated enhanced sensitivity, a wide detection range, low detection limit, rapid response, and long-term stability. Moreover, it was envisioned that the micro-structured sensor could have outstanding practicability when detecting diversified body movements. To demonstrate this, the sensor was firmly attached to various body parts of a healthy 26 years old volunteer to collect the capacitance signals in response to the body movements (Fig. 5a). The regular and repetitive output of the electrical signal could be observed when the
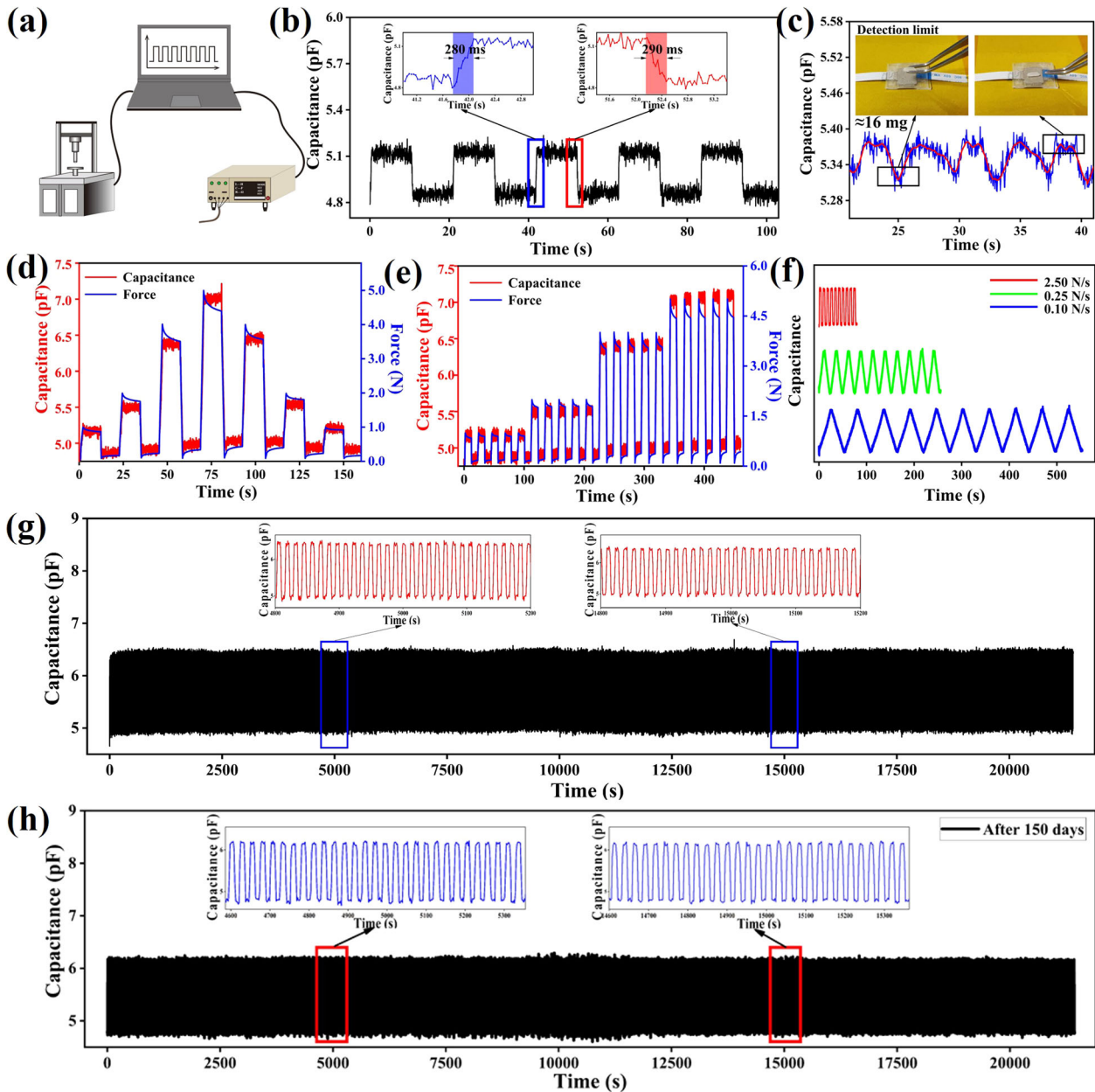
Fig. 4 Electron-mechanical characteristics of the flexible capacitance sensor. a Schematic diagram of the testing platform; **b** Response time of the sensor with the insets corresponding to the loading and unloading process; **c** Detection limit test by loading/unloading a grain of rice with a weight of 16 mg; **d** Capacitance change with the gradient increase and decrease under 10–45 kPa; **e** Cyclic capacitance changes under 10–45 kPa at the same frequency; **f** Ten cycles of the sensor with different loading speeds; **g**, **h** Stability test of the sensor under 40 kPa before and after 150 days; the insets are partially magnified curves for different cycle stages.

volunteer repeatedly pronounced the word "studying" (Fig. 5b), caused by the neck muscle movement and the vocal cord vibration. When the sensor was attached to the cheek, the stress of the air blowing on the device were distinctly responded (Fig. 5c). Furthermore, the stable capacitance change-time curves were obtained when the volunteer clenched and released his fist attached by the micro-structured sensor (Fig. 5d). The sensor was also capable of monitoring other body movements, such as the bending of the finger, elbow, and knee. The favorable reversibility during each testing cycle was achieved (Fig. 5e, f, g). Additionally, the angle recognition of the sensor was also demonstrated by attaching the sensor to the index finger (Fig. S10). When the sensor was placed on the sole, the highly stable signal output illustrated that the sensor could be used to monitor the response

to walking (Fig. 5h). As a result, the sensor's function of efficiently detecting diverse body movements within a broad detection range was proven.

The sensor was fixed on the surfaces of different objects to measure the sensing capability of the device as a tactile sensor in specific activities (Fig. 6). The stable electrical signals responding to the repeated quick touching and weight pressing on the sensor reflected the rapid response and good mechanical stability of the sensor (Fig. 6a, b). The sensor was also adhered to the beaker and keyboard to monitor the real-time grasping and knocking, which indicated the stable wave-forms and constant capacitance variations in response to the repeated actions (Fig. 6c, d). Figure 6e displays the signal output of the pressure sensor in response to a noncontact force from air blowing of aurilave. The sharp and
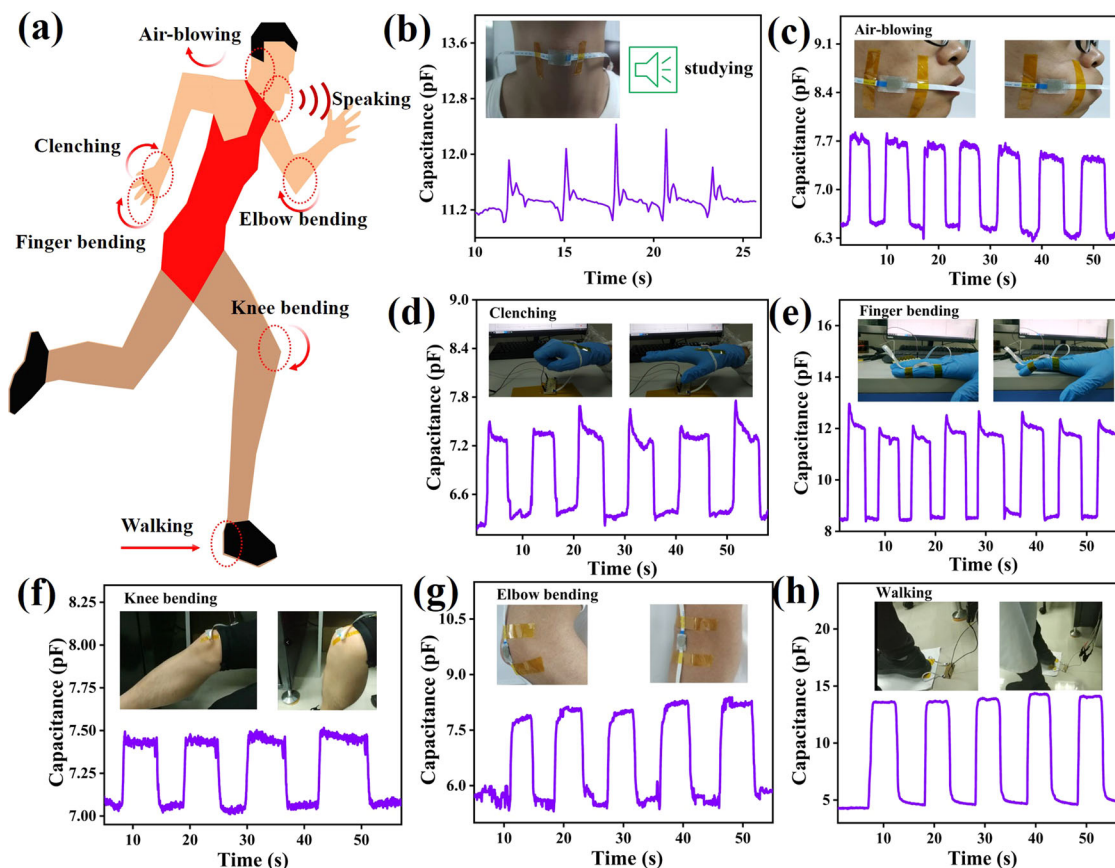
Fig. 5 Demonstration of the micro-structured sensor in response to human activities. a Schematic diagram of the sensor that detects human physiological signals and body motions; **b** Detection of the vocal cord vibration signal sent from the pronunciation of the word "studying"; **c–h** The capacitance responses come from the repeated air blowing, clenching and releasing of finger/knee/elbow bending, and walking.

repeated wave-forms reflected the high sensitivity and fast response of the sensor when detecting the real-time wind pressure. To assess the detection capability under high pressure, the six independent sensors were fabricated into an array to evaluate the volunteer's foot pressure distribution (Fig. 6f). The distinct capacitance values indicated that the sensor array could distinguish different parts of foot pressure when the volunteer was standing. Strike tests of the sensor at different pressures disclosed that the device rapidly responded to the repeatedly strong strikes by the fingertip, stainless cone, and pen point (Fig. 6g–i).

These results demonstrated the outstanding sensing ability of the micro-structured sensor to monitor diverse human activities and physical stimuli, accompanied by the characteristics of high sensitivity, fast response, excellent stability, and broad detection range. The synergy of the rough surface of the conductive materials and the nanoscale-microstructure of the dielectric layer contributed to the improvement of the sensor performance. The proposed sensor shows good prospects in healthcare, soft robots, human–machine interaction, and wearable devices.

METHODS

Synthesis of Ag NWs and MXene

A hydrothermal method was used for preparing Ag NWs according to our previous work[56,57]. First, 0.788 g silver nitrate, 0.53 g glucose, and 0.23 g ferric sulfate were dissolved in 100 mL distilled water to obtain a light-yellow solution. Second, 4.5 g poly(vinyl pyrrolidone) (K30) was added to the above solution under magnetic stirring for 2 h. Third, the

homogeneous mixture was transferred to a Teflon autoclave of 100 mL, and then heat-treated at $180\,^{\circ}C$ for 9 h. Finally, the gray-green Ag NWs were collected by repeated centrifugation and then dispersed in ethanol. $Ti_3C_2T_x$ was synthesized by a selective Al etching of MAX phase precursor powder (Ti_3AlC_2, 11 Technology Co., Ltd., China) by a minimally intensive layer delamination method. First of all, 1.6 g LiF was dissolved in 9 M HCl of 20 mL, and then 1 g Ti_3AlC_2 powder was added to LiF/HCl solution with the assistance of magnetic stirring to avoid a sharp increase in the reaction temperature. The etching reaction occurred at $35\,^{\circ}C$ for 48 h with the persistent stir. Subsequently, deionised water was used for washing the etched product until the pH value of the supernatant reached 6. Finally, the $Ti_3C_2T_x$ dispersion was ultra-sonicated for 2 h under the condition of the ice bath and Ar atmosphere. The delaminated $Ti_3C_2T_x$ flakes were collected from the upper solution.

Fabrication of micro-structured PDMS dielectric layer

The microstructure of the PDMS (Sylgard 184, Dow Corning) dielectric layer was replicated from the ESIM. First, the ESIM was peeled and then cleaned with deionised water. Second, the mixture of PDMS pre-polymer and a curing agent (10:1 by weight) was dropped on the dried ESIM surface. Finally, after cured at a temperature of $60\,^{\circ}C$ for 4 h, the ESIM was removed to obtain the PDMS dielectric layer with the inverted microstructure of the ESIM surface.

Construction of capacitive pressure sensor

The flexible capacitive pressure sensor was assembled based on a typical sandwich structure. The mixture of the fabricated Ag NWs and MXene (5:1 by weight) was firstly vacuum-filtrated on a filter membrane, and then we poured the mixture of PDMS pre-polymer and a curing agent (10:1 by weight) onto the MXene/Ag NWs-filter membrane. After cured at a
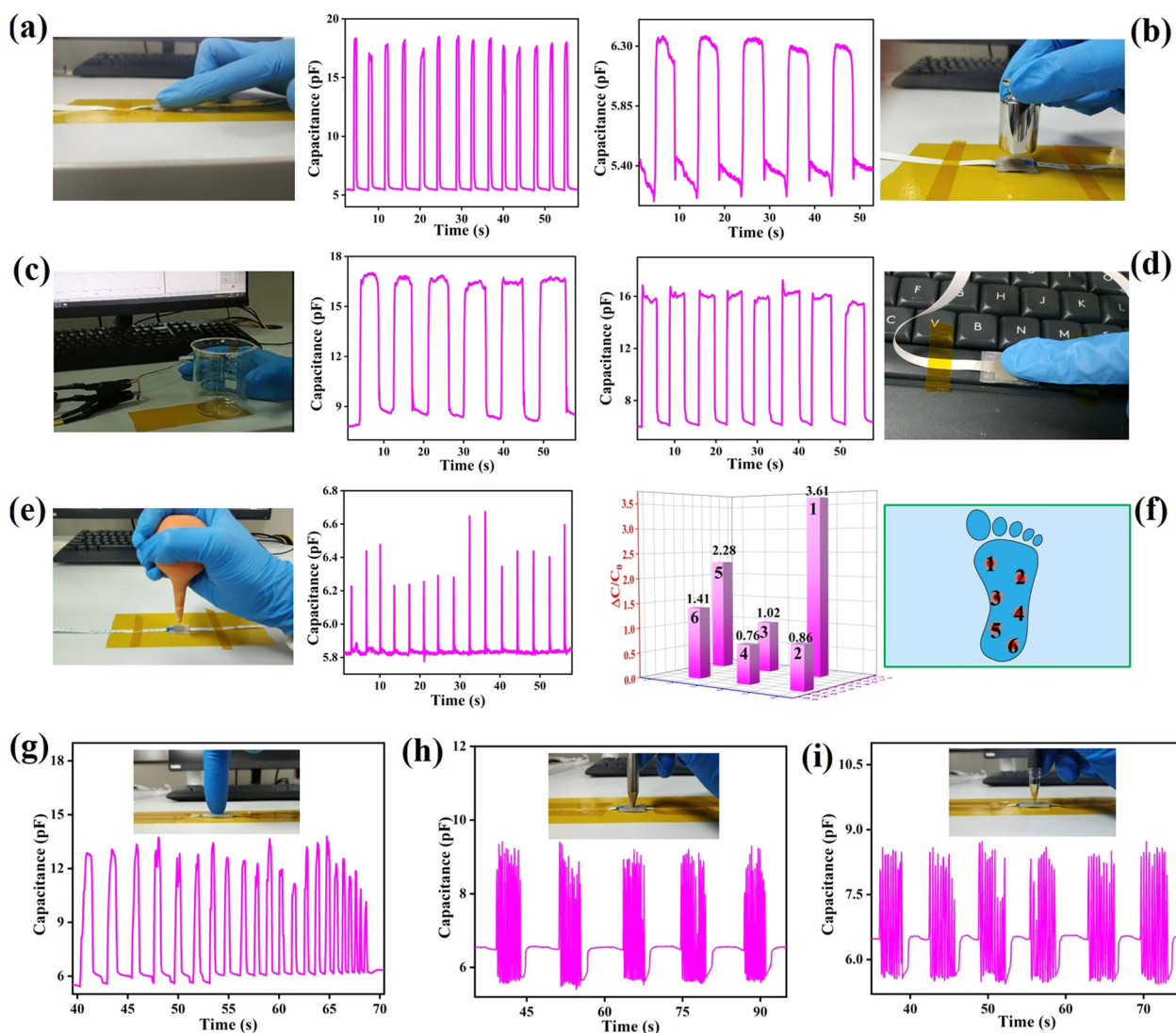
Fig. 6 Demonstration of the micro-structured sensor in response to exerted pressures. a, b Capacitance response of the sensor to quick touching and weight pressing; **c–e** Detection of various repeated actions, including grasping the beaker, knocking the keyboard, and blowing air; **f** Foot pressure distribution identified by a sensor array; **g–i** Detection of the repeated strikes of the sensor by the fingertip, stainless cone, and pen point.

temperature of 60 °C for 4 h, the composite conducting materials are embedded into the PDMS layer. The MXene/Ag NWs was completely transferred to the PDMS surface by removing the filter membrane, acquiring the electrodes. Finally, the electrodes and dielectric layer were cut with an area of 10 mm × 10 mm and then integrated into a sandwiched device. For performance comparison, we fabricated a flat sensor by using the same MXene/Ag NWs composite electrodes and a flat PDMS dielectric layer.

Characterization

A field emission scanning electron microscope (FE-SEM, Zeiss Sigma 500, Germany) was used for observing the morphology of the dielectric layer and electrode materials. The composition of the conductive materials was characterized through an X-ray diffractometer (XRD, X'pert Pro MFD, Panalytical, The Netherlands) with a Cu Kα radiation ($\lambda = 1.54178$ Å). The thickness of MXene sheets was determined by an atomic force microscope (AFM, MultiMode 8, Bruker, Germany). The surface potential of the conductive materials was tested using a Malvern Zetasizer (Nano ZS, England). The stress was applied to the sensors by a push-pull force gauge (LE, LiShi, China). The response performance of the stress-dependent sensor was evaluated by measuring the real-time capacitance changes of the device by an LCR (Inductance, Capacitance, Resistance) measurement instrument (IM3526, Rizhi, Japan). The capacitance of the sensor was tested under the frequency of 500 kHz.

In order to more accurately evaluate the advantage of the micro-structure in the flexible capacitive sensor, the FEA was conducted to compare the two models based on the micro-structured and planar PDMS dialectic layer by a commercial package Comsol 5.4. The micro-structured model was constructed according to the actual replicated surface of the dielectric layer with the electrodes replaced by the metal plates.

DATA AVAILABILITY

The data that support the findings of this study are available from the corresponding author upon reasonable request.

REFERENCES

1. Ohayon, D. & Inal, S. Organic bioelectronics: from functional materials to next-generation devices and power sources. *Adv. Mater.* **32**, 2001439 (2020).

2. Shi, X. et al. Bioinspired ultrasensitive and stretchable MXene-based strain sensor via nacre-mimetic microscale "brick-and-mortar" architecture. *ACS Nano* **13**, 649–659 (2018).

3. Honda, S. et al. Textile-based flexible tactile force sensor sheet. *Adv. Funct. Mater.* **29**, 1807957 (2019).

4. Liu, X. et al. Bio-inspired, micro-structured silk fibroin adhesives for flexible skin sensors. *ACS Appl. Mater. Interfaces* **12**, 5601–5609 (2020).

5. Li, F. et al. Printable and stretchable temperature-strain dual-sensing nanocomposite with high sensitivity and perfect stimulus discriminability. *Nano Lett.* **20**, 6176–6184 (2020).

6. Alam, M. M. et al. Ultra-flexible nanofiber-based multifunctional motion sensor. *Nano Energy* **72**, 104672 (2020).

7. Wu, X. et al. Large-area fabrication of high-performance flexible and wearable pressure sensors. *Adv. Electron. Mater.* **6**, 1901310 (2020).

8. Tang, X. et al. Multilevel microstructured flexible pressure sensors with ultrahigh sensitivity and ultrawide pressure range for versatile electronic skins. *Small* **15**, 1804559 (2019).

9. Zhu, G. J. et al. A highly sensitive and broad-range pressure sensor based on polyurethane mesodome arrays embedded with silver nanowires. *ACS Appl. Mater. Interfaces* **12**, 19988–19999 (2020).

10. Cheng, Y. et al. Bioinspired microspines for a high-performance spray $Ti_3C_2T_x$ MXene-based piezoresistive sensor. *ACS Nano* **14**, 2145–2155 (2020).

11. Liu, Q. et al. Highly transparent and flexible iontronic pressure sensors based on an opaque to transparent transition. *Adv. Sci.* **7**, 2000348 (2020).

12. Xiong, Y. et al. A flexible, ultra-highly sensitive and stable capacitive pressure sensor with convex microarrays for motion and health monitoring. *Nano Energy* **70**, 104436 (2020).

13. Bai, N. et al. Graded intrafillable architecture-based iontronic pressure sensor with ultra-broad-range high sensitivity. *Nat. Commun.* **11**, 209 (2020).

14. Hosseini, E. S., Manjakkal, L., Shakthivel, D. & Dahiya, R. Glycine-chitosan-based flexible biodegradable piezoelectric pressure sensor. *ACS Appl. Mater. Interfaces* **12**, 9008–9016 (2020).

15. Duan, S., Wu, J., Xia, J. & Lei, W. Innovation strategy selection facilitates high-performance flexible piezoelectric sensors. *Sensors* **20**, 2820 (2020).

16. Jung, Y. H. et al. Flexible piezoelectric acoustic sensors and machine learning for speech processing. *Adv. Mater.* **32**, 1904020 (2020).

17. Lou, M. et al. Hierarchically rough structured and self-powered pressure sensor textile for motion sensing and pulse monitoring. *ACS Appl. Mater. Interfaces* **12**, 1597–1605 (2020).

18. He, F. et al. Stretchable, biocompatible, and multifunctional silk fibroin-based hydrogels toward wearable strain/pressure sensors and triboelectric nanogenerators. *ACS Appl. Mater. Interfaces* **12**, 6442–6450 (2020).

19. Pyo, S., Choi, J. & Kim, J. Flexible, transparent, sensitive, and crosstalk-free capacitive tactile sensor array based on graphene electrodes and air dielectric. *Adv. Electron. Mater.* **4**, 1700427 (2018).

20. Choi, J. et al. Synergetic effect of porous elastomer and percolation of carbon nanotube filler toward high performance capacitive pressure sensors. *ACS Appl. Mater. Interfaces* **12**, 1698–1706 (2020).

21. Sharma, S., Chhetry, A., Sharifuzzaman, M., Yoon, H. & Park, J. Y. Wearable capacitive pressure sensor based on MXene composite nanofibrous scaffolds for reliable human physiological signal acquisition. *ACS Appl. Mater. Interfaces* **12**, 22212–22224 (2020).

22. Zhao, S. et al. 3D dielectric layer enabled highly sensitive capacitive pressure sensors for wearable electronics. *ACS Appl. Mater. Interfaces* **12**, 32023–32030 (2020).

23. Zhou, Q. et al. A bio-inspired cilia array as the dielectric layer for flexible capacitive pressure sensors with high sensitivity and a broad detection range. *J. Mater. Chem. A* **7**, 27334–27346 (2019).

24. Ma, L. et al. A highly sensitive and flexible capacitive pressure sensor based on a micro-arrayed polydimethylsiloxane dielectric layer. *J. Mater. Chem. C* **6**, 13232–13240 (2018).

25. Jian, M. et al. Flexible and highly sensitive pressure sensors based on bionic hierarchical structures. *Adv. Funct. Mater.* **27**, 1606066 (2017).

26. Wan, Y. et al. A highly sensitive flexible capacitive tactile sensor with sparse and high-aspect-ratio microstructures. *Adv. Electron. Mater.* **4**, 1700586 (2018).

27. Wan, Y. et al. Natural plant materials as dielectric layer for highly sensitive flexible electronic skin. *Small* **14**, 1801657 (2018).

28. Sun, X. et al. Carbon nanotubes reinforced hydrogel as flexible strain sensor with high stretchability and mechanically toughness. *Chem. Eng. J.* **382**, 122832 (2020).

29. He, Z. et al. Highly stretchable multi-walled carbon nanotube/thermoplastic polyurethane composite fibers for ultrasensitive, wearable strain sensors. *Nanoscale* **11**, 5884–5890 (2019).

30. Wang, Z. et al. High conductive graphene assembled films with porous microstructure for freestanding and ultra-low power strain sensors. *Sci. Bull.* **65**, 1363–1370 (2020).

31. Tian, H. et al. A graphene-based resistive pressure sensor with record-high sensitivity in a wide pressure range. *Sci. Rep.* **5**, 8603 (2015).

32. Bhattacharjee, M., Soni, M., Escobedo, P. & Dahiya, R. PEDOT:PSS microchannel-based highly sensitive stretchable strain sensor. *Adv. Electron. Mater.* **6**, 2000445 (2020).

33. Wang, Q. et al. Biocompatible, self-wrinkled, antifreezing and stretchable hydrogel-based wearable sensor with PEDOT:sulfonated lignin as conductive materials. *Chem. Eng. J.* **370**, 1039–1047 (2019).

34. Duan, S., Wang, Z., Zhang, L., Liu, J. & Li, C. A highly stretchable, sensitive, and transparent strain sensor based on binary hybrid network consisting of hierarchical multiscale metal nanowires. *Adv. Mater. Technol.* **3**, 1800020 (2018).

35. Cho, J. H., Ha, S. H. & Kim, J. M. Transparent and stretchable strain sensors based on metal nanowire microgrids for human motion monitoring. *Nanotechnology* **29**, 155501 (2018).

36. Kim, K.-H., Jang, N.-S., Ha, S.-H., Cho, J. H. & Kim, J.-M. Highly sensitive and stretchable resistive strain sensors based on microstructured metal nanowire/elastomer composite films. *Small* **14**, 1704232 (2018).

37. Li, T. et al. A flexible pressure sensor based on an MXene–textile network structure. *J. Mater. Chem. C* **7**, 1022–1027 (2019).

38. Yang, K. et al. A highly flexible and multifunctional strain sensor based on a network-structured MXene/polyurethane mat with ultra-high sensitivity and a broad sensing range. *Nanoscale* **11**, 9949–9957 (2019).

39. Guo, Y., Zhong, M., Fang, Z., Wan, P. & Yu, G. A wearable transient pressure sensor made with MXene nanosheets for sensitive broad-range human-machine interfacing. *Nano Lett.* **19**, 1143–1150 (2019).

40. Yuan, L. et al. Flexible and breathable strain sensor with high performance based on MXene/nylon fabric network. *Sens. Actuators A* **315**, 112192 (2020).

41. Wang, Y. et al. Rapid preparation of a Nafion/Ag NW composite film and its humidity sensing eeffect. *RSC Adv.* **10**, 27447–27455 (2020).

42. Zhang, S. et al. High conductive free-written thermoplastic polyurethane composite fibers utilized as weight-strain sensors. *Compos. Sci. Technol.* **189**, 108011 (2020).

43. Xie, X. et al. A spirally layered carbon nanotube-graphene/polyurethane composite yarn for highly sensitive and stretchable strain sensor. *Compos. Part A* **135**, 105932 (2020).

44. Pu, J.-H. et al. Multilayer structured AgNW/WPU-MXene fiber strain sensors with ultrahigh sensitivity and a wide operating range for wearable monitoring and healthcare. *J. Mater. Chem. A* **7**, 15913–15923 (2019).

45. Chen, M. et al. Self-assembly of dendritic-lamellar MXene/carbon nanotube conductive films for wearable tactile sensors and artificial skin. *Carbon* **164**, 111–120 (2020).

46. Zeng, X. et al. Tunable, ultrasensitive, and flexible pressure sensors based on wrinkled microstructures for electronic skins. *ACS Appl. Mater. Interfaces* **11**, 21218–21226 (2019).

47. Saqib, Q. M., Khan, M. U. & Bae, J. Inner egg shell membrane based biocompatible capacitive and piezoelectric function dominant self-powered pressure sensor array for smart electronic applications. *RSC Adv.* **10**, 29214–29227 (2020).

48. Gao, Y. et al. Microchannel-confined MXene based flexible piezoresistive multifunctional micro-force sensor. *Adv. Funct. Mater.* **30**, 1909603 (2020).

49. Lin, Z., Shao, H., Xu, K., Taberna, P.-L. & Simon, P. MXenes as high-rate electrodes for energy storage. *Trends Chem.* **2**, 654–664 (2020).

50. Zhang, J. et al. Scalable manufacturing of free-standing, strong $Ti_3C_2T_x$ MXene films with outstanding conductivity. *Adv. Mater.* **32**, 2001093 (2020).

51. Li et al. Hydrophobic and stable MXene-polymer pressure sensors for wearable electronics. *ACS Appl. Mater. Interfaces* **12**, 15362–15369 (2020).

52. Zhang, X. et al. Flexible MXene-decorated fabric with interwoven conductive networks for integrated joule heating, electromagnetic interference shielding, and strain sensing performances. *ACS Appl. Mater. Interfaces* **12**, 14459–14467 (2020).

53. Shen, G. et al. Transparent and stretchable strain sensors with improved sensitivity and reliability based on Ag NWs and PEDOT:PSS patterned microstructures. *Adv. Electron. Mater.* **6**, 2070034 (2020).

54. Sarycheva, A. & Gogotsi, Y. Raman spectroscopy analysis of the structure and surface chemistry of $Ti_3C_2T_x$ MXene. *Chem. Mater.* **32**, 3480–3488 (2020).

55. Ma, W., Yang, K., Wang, H. & Li, H. Poly(vinylidene fluoride-co-hexafluoropropylene) -MXene nanosheet composites for microcapacitors. *ACS Appl. Nano Mater.* **3**, 7992–8003 (2020).

56. He, X. et al. A highly conductive, flexible, transparent composite electrode based on the lamination of silver nanowires and polyvinyl alcohol. *J. Mater. Chem. C* **2**, 9737–9745 (2014).

57. Liu, J. et al. A one-dimensional Ag NW@NiCo/NiCo(OH)$_2$ core–shell nanostructured electrode for a flexible and transparent asymmetric supercapacitor. *J. Mater. Chem. A* **7**, 8184–8193 (2019).

AUTHOR CONTRIBUTIONS

X.H. and G.C. designed this work and analyzed the data; Z.L., G.S., and X.H. fabricated, characterized the electrodes and devices; J.L., Y.Z., T.L., and J.H. discussed the results; Y.X., C.Z., and D.Y. involved in the analysis of characterization; X.H. and Z.L. wrote the manuscript; G.C. revised the manuscript. All authors read and approved the final manuscript.

COMPETING INTERESTS

The authors declare no competing interests.

ADDITIONAL INFORMATION

Supplementary information The online version contains supplementary material available at https://doi.org/10.1038/s41528-021-00114-y.

Correspondence and requests for materials should be addressed to X.H. or G.C.

Reprints and permission information is available at http://www.nature.com/reprints

Publisher's note Springer Nature remains neutral with regard to jurisdictional claims in published maps and institutional affiliations.